Atmospheric Environment 212 (2019) 96–105

Contents lists available at ScienceDirect

Atmospheric Environment

journal homepage: www.elsevier.com/locate/atmosenv

Isotope-based source apportionment of nitrogen-containing aerosols: A case study in an industrial city in China

Mei-Yi Fan[a,b], Yan-Lin Zhang[a,b,*], Yu-Chi Lin[a,b], Yun-Hua Chang[a,b], Fang Cao[a,b], Wen-Qi Zhang[a,b], Yong-Bo Hu[a,b], Meng-Ying Bao[a,b], Xiao-Yan Liu[a,b], Xiao-Yao Zhai[a,b], Xin Lin[a,b], Zhu-Yu Zhao[a,b], Wen-Huai Song[a,b]

aYale-NUIST Center on Atmospheric Environment, International Joint Laboratory on Climate and Environment Change (ILCEC), Nanjing University of Information Science & Technology, Nanjing, 210044, China

[b] *Key Laboratory of Meteorological Disaster, Ministry of Education (KLME)/ Collaborative Innovation Center on Forecast and Evaluation of Meteorological Disasters (CIC-FEMD), Nanjing University of Information Science & Technology, Nanjing, 210044, China*

GRAPHICAL ABSTRACT

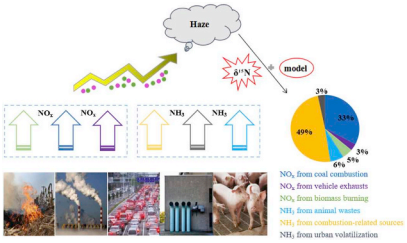

ARTICLE INFO

Keywords:
Nitrogen-containing aerosols
Aerosol liquid water content
Optimized Bayesian isotope mixing model

ABSTRACT

Due to the local emissions and transportations of air pollution from the most polluted regions such as the North China Plain and Yangtze Delta metropolitan, Xuzhou is becoming one of the most polluted cities in East China. The sources and formation processes of nitrogen-containing aerosols are therefore very complex. Two continuous aerosol measurement campaigns were conducted in this industrial city during the wintertime and summertime of 2016, to investigate the chemical compositions and potential sources of total nitrogen (TN, including 89% inorganic nitrogen and 11% organic nitrogen) in $PM_{2.5}$. Abrupt enhancements of nitrogen-containing aerosols (e.g., NO_3^- and NH_4^+) were found in the winter, and nitrate became as a dominant contributor in high pollution days (e.g., $PM_{2.5} > 150\,\mu g\,m^{-3}$). Nitrogen oxidation ratios (NOR) correlated significantly with aerosol liquid water content (ALWC), which was estimated by ISORPROPIA-II model. This suggested heterogeneous process might be an important pathway in nitrate formation during the high $PM_{2.5}$ days. The nitrogen isotope composition ($\delta^{15}N$) in TN varied from −1.3 to +13.2‰ with a mean value of 6.9 ± 3.6‰ during the wintertime. An isotope-based source apportionment approach was then developed using a Bayesian isotope mixing model (SIAR) with chemical compositions as an important constrain, which improved accuracy and reduced the overall uncertainties in estimations of TN sources. From this optimized model, we identified six major sources including NH_3 from combustion-related emissions (49%), NH_3 derived from animal wastes (6%), NH_3 from urban volatilization (3%), NO_x derived from coal combustion (33%), NO_x from biomass burning (5%) and NO_x from vehicles (3%). Our results demonstrated that ambient NO_x was dominated by coal combustion. Since NO_x and NH_3 are important precursors for ammonium nitrate aerosols, controlling of combustion related NO_x and NH_3 emissions might be an important way to reduce $PM_{2.5}$ levels in this region.

* Corresponding author. Yale-NUIST Center on Atmospheric Environment, International Joint Laboratory on Climate and Environment Change (ILCEC), Nanjing University of Information Science & Technology, Nanjing 210044, China.
E-mail addresses: zhangyanlin@nuist.edu.cn, dryanlinzhang@outlook.com (Y.-L. Zhang).

https://doi.org/10.1016/j.atmosenv.2019.05.020
Received 9 October 2018; Received in revised form 5 May 2019; Accepted 11 May 2019
Available online 15 May 2019
1352-2310/

1. Introduction

Airborne particulate matter (PM) with an aerodynamic diameter less than 2.5 μm ($PM_{2.5}$) has huge impact not only on air quality, but also on radiative forcing and climate change (Booth and Bellouin, 2015; Che et al., 2014; Wang et al., 2014). It also has adverse effects on human health because of its easy inhalation and deposition to human's lungs, causing illness such as asthma, bronchitis and cardiovascular disease (Peplow, 2014; Cao et al., 2014; Ouyang, 2013; Mukherjee et al., 2017).

China has been experiencing a severe PM pollution problem due to increasing consumptions in fossil fuel. Although the China government has made big efforts in reducing anthropogenic emissions for many years, a lot of PM haze events still occurred, especially in some industrial cities and metropolitan areas like Beijing, Shanghai, Nanjing and Hangzhou (Cheng et al., 2017; Tan et al., 2018; Wu et al., 2016; Zhang et al., 2017). Previously, numerous studies suggested that the formation of PM haze were attributed to high concentrations of gaseous precursors (such as NO_x and SO_2), stagnant conditions (weak wind speed, high relative humidity) and temperature inversion which were favorable for the accumulation of airborne PM (Zhang et al., 2009; Petäjä et al., 2016; Xu et al., 2017a). During haze events, apparent enhancements of secondary inorganic aerosols (SIA) and aerosol liquid water content (ALWC) were usually observed (Sun et al., 2016; Lin et al., 2014; Sulong et al., 2017). The aqueous-phase reactions of NO_x and SO_2 on ALWC trigger formation of SIA and were considered as major mechanisms for increasing SIA concentrations in the atmosphere, especially in haze events (Pathak et al., 2009; Cheng et al., 2016; Xu et al., 2017b).

Particulate total nitrogen (TN) exist mainly as forms of NH_4^+-N and NO_3^--N in the atmosphere. Both nitrogen-containing species are major compositions of secondary inorganic aerosols; the abundances of these nitrogen species in SIA were in a range of 14–66% in polluted air (Tao et al., 2018; Jiang et al., 2018; Liang et al., 2017). With significant reduction of SO_2 emissions and fast growth of vehicles emissions, $PM_{2.5}$ in China has been changed from sulfate-enriched PM to nitrate-dominated PM in the recent years (Pan et al., 2016). In other works, nitrogen-containing aerosols has become the major contributor to $PM_{2.5}$, especially during haze events (Xu et al., 2017b; Li et al., 2017); therefore, estimation of particulate TN sources can provide insights to control the emissions for formation of nitrogen-containing aerosols and decrease PM levels.

Stable nitrogen isotope ($\delta^{15}N$) technique has been used to track the potential sources of atmospheric nitrogen (Wang et al., 2017). Utilization $\delta^{15}N$ values determined in nitrogen-containing aerosols and their precursors (NH_3 and NO_x), the potential sources of particulate TN can be estimated (Aggarwal et al., 2012; Hegde et al., 2016). The isotope fractionation effect occurred during the exchange processes of gas to aerosol-phase processes; resulted in influence the $\delta^{15}N$ in atmospheric particulates. Previous studies showed that the isotopic fractionation effects between NH_3 and NH_4^+ are more significant than that between NO_2 and aerosol N (Kawashima and Kurahashi, 2011). In this study, we will use an optimized Bayesian isotope mixing model based on $\delta^{15}N$-TN values after considering fractionation effect between gas NO_x (NH_3) and aerosol NO_3^- (NH_4^+) to quantify the sources of airborne particulate TN.

Xuzhou, one of the heavy polluted industrial cities in the southern part of North China Plain (NCP), has been experiencing poor air quality for a long time due to its rapid industrialization. In this work, daily $PM_{2.5}$ samples were collected in Xuzhou during the winter and summer periods in the year of 2016. Water soluble ions, total nitrogen (TN) along with $\delta^{15}N$ in $PM_{2.5}$ samples were determined. Apart from characterizing the water soluble ions in airborne $PM_{2.5}$ in this industrial city during the different seasons, we also provided some insights of evolutions for water soluble ions and TN during the high PM levels. Meanwhile, factors affecting on formation of airborne nitrogen-containing aerosols and potential sources for particulate TN in high PM days were also identified using nitrogen isotope techniques.

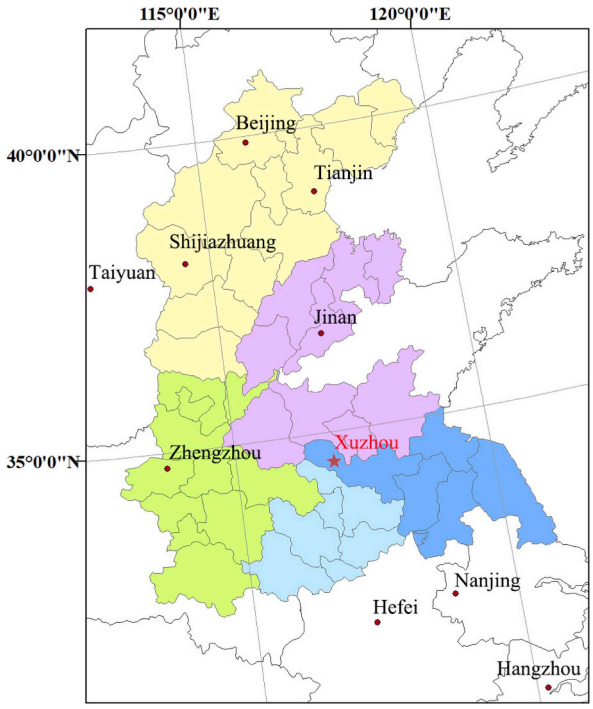

Fig. 1. Sampling site in this study.

2. Methods

2.1. Sampling

Daily $PM_{2.5}$ sampling was carried out in Xuzhou, a typically industrial city located in the southern part of NCP, with an area of 11,258 km^2 and a population of over 8 million. The aerosol sampling site was located at the rooftop (approximately 30 m above ground) of the Maintenance Branch Office of State Grid (34°11′N, 117°16′E), which was a suburb area mixed commercial and residential area (Fig. 1). Vehicular and resident activities are the major emission sources surrounding the sampling site.

During the sampling periods, daily aerosol samples were collected on pre heated (ie.,450 °C for 6 h) 8 × 10 inch quartz microfiber filters (PALL, USA) through a high volume aerosol sampler (KC-1000, Laoshan Mountain Electronic Instrument Factory, flow rate:1.05 $m^3\,min^{-1}$) equipped with a 2.5 μm cut-off size inlet from January 6 to February 17 (defined as the wintertime) and August 1 to 30, 2016 (defined as the summertime). During the sampling process, two blank filters were put on the sampling holder for 1 min with pump off, in order to deduct the influence of the field environment on the actual collection of aerosol samples. After sampling, the filtered samples were placed into aluminum foils, sent back to laboratory and placed in petri dishes desiccator maintained at 21 ± 2 °C temperature and 40 ± 5% relative humidity for 72 h to remove the moisture. Subsequently, the filters were stored in the refrigerator with a temperature of −20 °C before chemical analysis.

2.2. Analysis methods

Gravimetric method was used to estimate $PM_{2.5}$ mass concentrations. An electronic microbalance (Sartorius BSA124S, sensitivity: 0.1 mg) was applied to weight the mass of filters before and after sampling under certain conditions with relative humidity (RH) of ~40% and temperature of 25 °C.

After sampling, two pieces of 18 mm (2.54 cm^2) filters were punched, extracting with 30 mL ultra-pure water (Milli-Q Reference, America) for 30 min and then determined water soluble ions such as Cl^-, NO_3^-, SO_4^{2-}, Na^+, NH_4^+, K^+, Mg^{2+} and Ca^{2+} by ion chromatography (IC, ICS 5000+, Thermo Scientific). There were two systems for determination of cations (eluent: 20 mmol L^{-1} methane sulfonic acid (MSA); guard column: CG12A 4 mm; separation column: CS12A 4 mm; Suppressor: CERS500 4 mm) and anions (eluent: 50 mM NaOH and ultra-pure water; guard column: AG11 HC 4 mm; separation column: AS11 HC 4 mm; suppressor: AERS500 4 mm) in aerosol samples. In terms of QA/QC procedures, eight-point calibration curves, including 0.05, 0.1, 0.2, 0.5, 1, 2, 5, and 10 ppm were made for each batch of samples and the correlation coefficients of the calibration curves were all greater than 0.999. The precisions of all species were less than 2% and the average recoveries for all species appeared in the range from 90% to 110%. The MDLs calculated as three times the standard deviation of blanks were 0.12, 0.21, 0.26, 0.12, 0.41, 0.03, 0.08 and 0.03 ng m^3 for Na^+, NH_4^+, Mg^{2+}, K^+, NH_4^+, Ca^{2+}, Cl^-, NO_3^- and SO_4^{2-}.

Concentrations of TN and $\delta^{15}N$ values in $PM_{2.5}$ were analyzed using the element analyzer (EA, FLASH, 2000; Thermo Fisher Scientific) combined with an isotope ratio mass spectrometer (MAT253, Thermo Fisher Scientific). A small disc (area 1.53 cm^2) of each sampled filter was cut out and put into a tin cup. The tin cups were shaped into rounded balls using a pair of flat-tipped tweezers and put into the autosampler of EA. The samples were oxidized in a combustion column packed with chromium trioxide at 1020 °C. The tin container burns to promote the intensive oxidation of sample materials in an atmosphere of pure oxygen, and then the combustion products were transferred to a reduction column packed with metallic copper under the constant level of temperature at 650 °C. In this process, excess oxygen was removed and nitrogen oxides were reduced to molecular nitrogen (N_2). The N_2 derived during this process was isolated on-line using a gas chromatograph and then measured with a thermal conductivity detector. Aliquots of the N_2 gases were then introduced into the isotope ratio mass spectrometer through an interface. Acetanilide#1 ($\delta^{15}N$: 1.18‰) and Acetanilide#2 ($\delta^{15}N$: 19.56‰) were used as the external standards to determine TN and its isotopic ratio. Isotope ratio ($\delta^{15}N$) values were presented as parts per thousand relevant to standards (Wang et al., 2017):

$$\delta^{15}N = (R_{sample}/R_{standard}\text{-}1) \times 1000 \quad (1)$$

$$R = {}^{15}N/{}^{14}N \quad (2)$$

where R_{sample} was the isotope value of sample and $R_{standard}$ was the isotope value of atmosphere N_2.

To verify the losses of ions on filters during drying process in the dish, seven filters representing different degree of pollution were chose for NO_3^- (NH_4^+) concentration measurement to evaluate the loss before and after drying due to volatilization or bacterial consumption. The result in Fig. S1 showed there almost no difference of NO_3^- (NH_4^+) concentrations before and after drying. Moreover, we also compared the $\delta^{15}N$-TN values of these filters, and the result indicated drying process did not cause changes in isotope values as showed in Fig. S2.

2.3. Calculation of aerosol liquid water content

ISORROPIA-II model, a thermodynamic equilibrium model for the Na^+ - Cl^- - Ca^{2+} - K^+ - Mg^{2+} - SO_4^{2-} - NH_4^+ - NO_3^- - H_2O aerosol system (Fountoukis and Nenes, 2007), was used to calculate aerosol liquid water content (ALWC). Previous studies showed the ALWC predicted values using ISORROPIA-II model were in a good agreement with those of field measurements (Bian et al., 2014; Guo et al., 2015). Due to the lack of NH_3 measurement, the model was set up to solve "reverse" scheme with the chemical species in the metastable state. Particulate organic matter was not considered participating in the calculation of ALWC because of the mass fraction of organic matter-induced particle water accounted for a few percent of total ALWC (Xue et al., 2016). Apart from aforementioned ionic species, relative humidity and ambient temperature were also served as input parameters for ISORROPIA-II model simulations.

2.4. Meteorology and gases data

Meteorological parameters during the sampling periods were obtained from China Meteorological Data Network of the National Meteorological Administration (http://www.cma.gov.cn/), mainly including ambient temperature (T) and relative humidity (RH). On the other hand, the data of gas pollutants (NO_2, SO_2, CO and O_3) were also obtained from the China Meteorological Data Network (http://data.cma.cn/).

2.5. Bayesian isotope mixing model

The Stable Isotope Analysis in the R (SIAR) model was used to

Table 1
Average concentrations of $PM_{2.5}$ mass, ionic species, TN and gaseous pollutants along with ambient temperature and relative humidity observed in Xuzhou during sampling period.

Component	Overall period	Winter	Range	Summer	Range	Winter/Summer
Number	57	27		30		
$PM_{2.5}$ (μg m^{-3})	136.8 ± 88.2	213.2 ± 52.1	150.6–350.5	66.5 ± 23.1	35.5–123.5	3.2
Temp (°C)	11.6 ± 15.2	0.6 ± 4.7	−10 - 4	30.9 ± 3.2	26–35	
RH (%)	65.9 ± 15.3	60.8 ± 14.9	32–94	75.1 ± 11.0	53–92	0.8
TN (μg m^{-3})	11.6 ± 9.4	18.7 ± 9.1	5.0–49.5	5.5 ± 2.3	2.2–11.5	3.4
NH_4^+ (μg m^{-3})	9.2 ± 7.1	14.1 ± 7.9	3.9–44.3	4.8 ± 1.8	2.0–9.8	2.9
NO_3^- (μg m^{-3})	14.3 ± 13.1	24.6 ± 11.8	5.2–55.9	4.9 ± 2.4	1.4–14.1	5.0
SO_4^{2-} (μg m^{-3})	14.9 ± 9.0	18.9 ± 11.6	5.5–66.2	11.4 ± 3.9	2.5–21.8	1.6
Ca^{2+} (μg m^{-3})	2.7 ± 2.4	4.2 ± 2.6	0.1–8.8	1.3 ± 0.9	0.1–3.6	3.2
K^+ (μg m^{-3})	2.0 ± 5.0	3.5 ± 6.6	0.5–29.2	0.4 ± 0.3	0.1–1.3	8.7
Cl^- (μg m^{-3})	3.3 ± 4.0	6.3 ± 3.8	0.9–19.8	0.5 ± 0.2	0.1–1.5	12.6
Na^+ (μg m^{-3})	0.4 ± 0.3	0.6 ± 0.3	0.2–1.6	0.2 ± 0.1	0.1–0.4	3.0
Mg^{2+} (μg m^{-3})[a]	0.2 ± 0.3	0.3 ± 0.4	< n.d. - 2.1	0.04 ± 0.04	< n.d. - 0.1	7.5
TWSIIs (μg m^{-3})	42.2 ± 34.1	72.9 ± 33.1	23.0–184.9	23.7 ± 7.56	7.56–45.0	3.1
SO_2 (ppb)	12.2 ± 4.4	12.6 ± 4.9	2.9–25.1	11.5 ± 3.8	4.9–21.1	1.1
NO_2 (ppb)	36.8 ± 17.0	44.5 ± 17.5	16.4–82.8	25.6 ± 7.4	17.4–48.3	1.7
CO (ppb)	1207 ± 547	1432 ± 601	460–2765	885.5 ± 190.9	609–1367	1.6
O_3 (ppb)	25.6 ± 12.6	17.9 ± 6.3	8.3–31.8	36.6 ± 11.2	21.3–58.3	0.5
LWC (μg m^{-3})	38.1 ± 37.5	48.8 ± 42.3	6.3–170.5	28.1 ± 29.8	3.1–135.0	1.7

[a] < n.d. Denotes the concentration below detection limit.

estimate the proportional contributions of various sources to bulk N in $PM_{2.5}$. This model ran a Bayesian isotope mixing model in the R software package to establish a logical prior distribution firstly and determine the probability distribution of the contribution of each source to the mixture (Evans et al., 2000). A set of N mixture measurements on j isotopes with k source contributors were defined to achieve the purpose of the mixing model (Parnell et al., 2010):

$$\begin{aligned} Xij &= \sum_{k=1}^{k} pk\,(Sjk + cjk) + \varepsilon ij \\ Sjk &\sim N\,(\mu jk,\ \omega_{jk}^2) \\ cjk &\sim N\,(\lambda jk,\ \tau_{jk}^2) \\ \varepsilon jk &\sim N\,(0,\ \sigma_j^2) \end{aligned} \quad (3)$$

where all p values sum to 1 (unity), X_{ij} is the isotope value j of the mixture i, in which $i = 1, 2, 3, \ldots, N$ and j = 1, 2, 3, …, J; S_{jk} is the source value k on isotope j ($k = 1, 2, 3, \ldots, K$) which is normally distributed with mean μ_{jk} and standard deviation ω_{jk}; p_k is the proportion of source k estimated by SIAR model; c_{jk} is the fraction factor for isotope j of source k and is normally distributed with λ_{jk} and standard deviation τ_{jk}; and ε_{ij} is the residual error representing the additional unquantified variation between individual mixtures, and is normally distributed with mean 0 and standard deviation σ_j. A more detailed description of this model can be found in Parnell et al. (2010). The SIAR model was applied to estimate the contributions of N sources in the $PM_{2.5}$ samples during winter ($n = 27$). One isotope ($j = 1$) ($\delta^{15}N$ of bulk N) was utilized and $\delta^{15}N$ values of each $PM_{2.5}$ sample were analyzed as one group.

3. Results and discussion

3.1. Chemical characteristics of $PM_{2.5}$

During the sampling periods, total of 57 aerosol samples were collected in Xuzhou; therein, 27 aerosol samples were collected in the wintertime and 30 samples were obtained in the summertime. Table 1 lists the concentrations of $PM_{2.5}$ mass and its chemical constituents together with gaseous pollutants. The average mass concentrations of $PM_{2.5}$ during the entirely sampling periods were 137 ± 88 μg m^{-3}. Compared to other cities in China, the level of $PM_{2.5}$ mass in Xuzhou was relatively high (see in Table 2), indicating that PM pollution is a serious problem in this city. In terms of TWSIIs, the average concentration was 42.2 ± 34.1 μg m^{-3}, accounting 36% for $PM_{2.5}$ mass. Sulfate was the most predominant species, which accounted for 32.1% of TWSIIs mass, followed by nitrate (29.8%), ammonium (19.4%) chloride (6.6%), calcium (5.7%) and potassium (4.1%). The average concentrations of TN varied from 2.2 to 49.5 μg m^{-3} with a mean value of 11.6 ± 9.4 μg m^{-3} which accounted 8% for $PM_{2.5}$ mass. Ammonium-N (NH_4^+-N) was the predominant N-containing species in the fine mode aerosols with an average concentration of 7.2 μg m^{-3}, accounting 62% for TN mass. Nitrate-N (NO_3^--N) averaged at 3.2 μg m^{-3} and occupied ~27% of TN concentration. The average concentration of organic nitrogen (ON) calculated by TN concentration subtracting the concentrations of NH_4^+-N and NO_3^--N was 1.3 μg m^{-3}, which accounted 11% for TN mass.

Significant differences of concentrations in $PM_{2.5}$ mass, TWSIIs and TN were found between the wintertime and summertime (see in Table 1). $PM_{2.5}$ mass concentrations in the wintertime (ranging from 151 to 351 μg m^{-3} with a mean value of 213 μg m^{-3}) were obviously higher than those in the summertime (ranging from 36 to 124 μg m^{-3} with a mean value of 67 μg m^{-3}). The similar results were also found for TWSIIs and TN. The average concentrations of TWSIIs and TN were 72.9 and 18.7 μg m^{-3} in the wintertime, which were, respectively, 3.1 and 3.4 times higher than those during the summer sampling period. The higher concentrations in the wintertime was probably attributed to the favorable conditions, such as stagnant and lower boundary layer, for accumulation of air pollutants, resulting in increasing concentrations of $PM_{2.5}$ mass, TWSIIs and TN in the atmosphere.

For ionic species, the winter-to-summer ratios of main ionic concentrations were in the order of Cl^- (12.6) > K^+ (8.7) > NO_3^- (5.0) > Ca^{2+} (3.2) > NH_4^+ (2.9) > SO_4^{2-} (1.6). The substantial increases of Cl^- and K^+ concentrations in the wintertime were presumably due to the biomass burning (BB) emissions since both species are indicators for BB activities (Pósfai et al., 2003). Nitrate and ammonium, both are major airborne nitrogen species, also exhibited higher concentrations in the winter with the winter-to-summer ratios of 5.0 and 2.9, respectively, which were much higher than that of sulfate (1.6). Such similar phenomena, that is, rapid increasing rates of nitrate and ammonium than that of sulfate during polluted seasons was also founded in Beijing, Shanghai and Hangzhou (Tan et al., 2018; Pan et al., 2016b; Cheng et al., 2017; Wu et al., 2016). The significant enhancements of NO_3^- and NH_4^+ might be explained by more NH_4NO_3 formation under the low ambient temperature condition which will be discussed in section 3.2. Moreover, the average concentration of Ca^{2+} during the wintertime was 4.2 ± 2.6 μg m^{-3}, exceeding that (1.3 ± 0.9 μg m^{-3}) in the summer by a factor of 3.2. The elevated Ca^{2+} in the wintertime might be due to dust particles passed over the sampling site (Taghvaee et al., 2018). In case of ALWC, the average concentration in the winter was 48.8 ± 42.3 μg m^{-3}, which was 2 times higher than that in the summer (28.1 ± 29.9 μg m^{-3}). The higher ALWC in the wintertime might be associated with the higher concentrations of SIA since they are hygroscopic species.

3.2. Enhancements of nitrogen species during the wintertime

Fig. 2a illustrates the concentrations of water-soluble ions in different $PM_{2.5}$ levels during the sampling periods. As expected, the concentrations of all ionic species increased profoundly with increasing $PM_{2.5}$ mass. The relative abundances of ions in TWSIIs dependent on $PM_{2.5}$ levels are plotted in Fig. 2b. Although the sulfate concentrations increased considerably in the high $PM_{2.5}$ levels ($PM_{2.5}$ > 150 μg m^{-3}), the relative abundances kept almost constant levels. However, for nitrogen species, significant enhancements during the high PM levels were found for both absolute concentrations and relative abundances, especially for nitrate. The abundance of nitrate was approximately 19% when $PM_{2.5}$ concentration was less than 150 μg m^{-3}; nevertheless, nitrate contribution was increased up to 37% with $PM_{2.5}$ exceeding 170 μg m^{-3}. This suggested that nitrate was a dominant contributed species during the high $PM_{2.5}$ days compared to sulfate and ammonium, and resulting in elevated TN concentration in the high $PM_{2.5}$ levels. In the atmosphere, nitrate is mainly existed in a form of ammonium nitrate (NH_4NO_3). There are several factors (e.g., gaseous precursors, ambient temperature and relative humidity) affecting on airborne

Table 2
Concentrations of $PM_{2.5}$ mass, water-soluble ions in different cities (unit:μg m^{-3}).

Cities	Sampling period	Sample number	$PM_{2.5}$	NH_4^+	K^+	Ca^{2+}	Cl^-	NO_3^-	SO_4^{2-}	SIA	References
Xuzhou	2016	57	136.8	9.2	2.0	2.7	3.3	14.3	14.9	38.4	This study
Shanghai	2013–2014	69	96.8	7.3	1.7	–	3.2	15.9	13.1	36.4	Ming et al. (2017)
Lin'an	2011	20	–	5.9	0.9	1.3	0.8	4.1	13.0	23.0	Li et al. (2015)
Nanjing	2013–2014	6727	96.6	23.4	2.0	0.6	4.4	22.3	32.2	77.8	Wang et al. (2016)
Hangzhou	2014–2015	Sampling once every 6 days	78.4	9.5	1.0	0.6	1.9	13.8	14.2	37.5	Xu et al. (2017a)

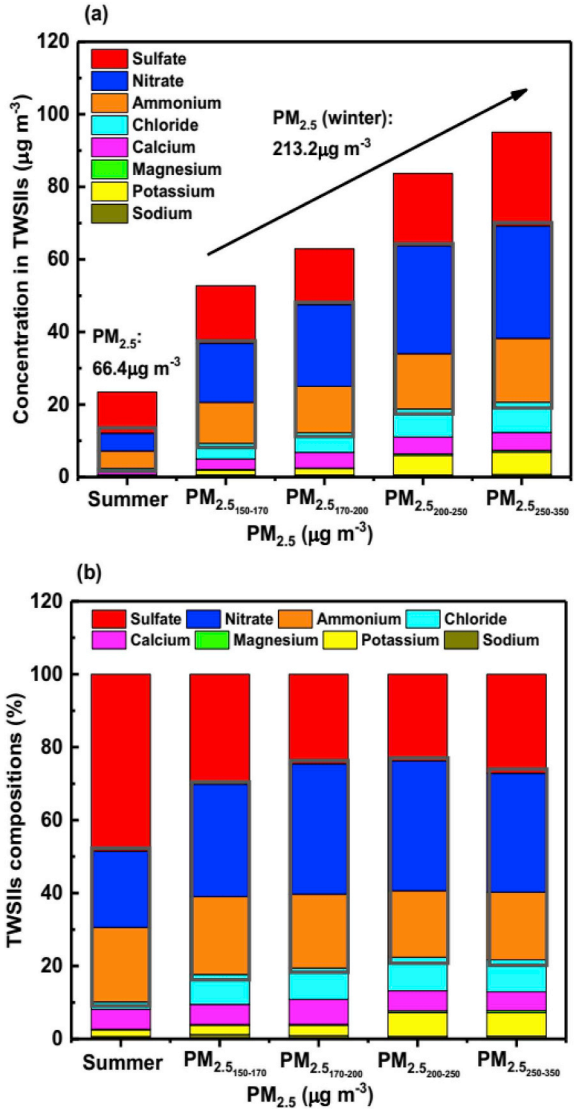

Fig. 2. (a) The concentrations and (b) abundances of ionic species in $PM_{2.5}$ in various PM pollution levels. In this figure, the gray blocks represent N-containing species.

particulate nitrate concentration and its formation. NO_x, mainly emitted from vehicle emissions and stationary sources, proceeds homogeneous (NO_2 + OH) and heterogeneous (N_2O_5 + H_2O) reactions to produce aqueous nitrate, and to be neutralized by NH_4^+. Thus, NO_2 and NH_3, precursors of NH_4NO_3, would influence the formation of particulate NH_4NO_3. On the other hand, formation of particulate NH_4NO_3 is very sensitive to ambient relative humidity and temperature (Lin and Cheng, 2007). Low temperature and high relative humidity are favorable conditions for yield of particulate NH_4NO_3. Carbon monoxide (CO), an indicator for vehicle emissions, is a relative stable gas in the atmosphere and therefore can be used to trace the behaviors for atmospheric conditions (Zhang et al., 2018). Assuming constant levels of emissions emitted from combustion sources during the sampling periods, we supposed that the increase of CO concentrations (see in Fig. 3d) in the wintertime was mainly caused by the lower boundary layer height. However, compared with the enhancements of CO (1.6) and NO_2 (1.7) in the winter, the increase of nitrate (5.0) was much more remarkable (see in Table 1 and Fig. 3). This suggested that the high concentration of nitrate in the winter was not only due to the decrease of boundary layer height, but also attributed to the increase concentration of NO_x and atmospheric process for nitrate formation. As mentioned above, formation of nitrate aerosols is very sensitive to RH and temperature, in particular, high temperature suppresses the formation of nitrate due to equilibrium between gas-phase and aerosol-phase nitrate and ammonium.

The ambient RH and temperature during the sampling periods are illustrated in Fig. 3a and b. In the wintertime, the ambient RH averaged at 61%, which was much lower than that 75% in the summer, indicating that low RH was not a reason for high nitrate levels in the cold season. On the contrary, the ambient temperature during the winter sampling period averaged at 0.6 °C, which was much lower than that (31 °C) in the summertime. High temperature inhibited NH_4NO_3 formation, causing lower nitrate concentrations in the warm season (Lin and Cheng., 2007). Therefore, high concentrations of particulate nitrate in the wintertime might be due to the lower temperature which favored the nitrate aerosol formation. Moreover, the high NO_x concentrations, implying higher precursors, was probably another reason for high nitrate concentrations in the wintertime.

3.3. Nitrogen oxidation ratio

Nitrogen oxidation ratio (NOR) was used to evaluate the degree of oxidation of NO_2 to particulate nitrate, which can be calculated by the following formula (Yang et al., 2017):

$$NOR = [NO_3^-]/([NO_2] + [NO_3^-]) \quad (4)$$

where NO_3^- and NO_2 are the concentrations with the units of μmol m^{-3}. In the wintertime, the average values of NOR was 0.24 exceeding that in the summertime (0.10) by a factor of 1.4, indicating that more NO_2 transformed to nitrate particles in the cold season. Our NOR values were in agreement with those calculated by Yang et al. (2017) who reported that the average NOR values in Handan were 0.26 and 0.09 during the wintertime and summertime, respectively. Fig. 4 illustrates the NOR depends on different ambient temperature, relative humidity and ALWC bin values. It is found that NOR seemed to be sensitive to ambient temperature and ALWC. For instance, when the ambient temperature was lower than 25 °C, the NOR values were above 0.2. Nevertheless, the NOR value decreased drastically to 0.1 as the temperature was higher than 25 °C. This supported the argument that temperature would restrict nitrate aerosol production. Interestingly, NOR values did not increase with relative humidity, but with ALWC concentrations. As mentioned above, the hydrolysis of N_2O_5 on pre-existing aerosols is an important formation mechanism of nitrate in polluted atmosphere in China (Pathak et al., 2009). The increase of NOR value coincided with increasing ALWC suggested that enhancements of nitrogen oxidation ratios in high ALWC concentrations; probably reflected that heterogeneous reaction was a major mechanism for nitrate aerosol formation in Xuzhou located in southern NCP region. This finding was consistent with the conclusion by Chang et al. (2018) who suggested that heterogeneous reaction was a major mechanism of nitrate aerosol formation in urban polluted air.

3.4. Source apportionment of TN in $PM_{2.5}$ during winter

As discussed above, TN concentrations increased evidently in the wintertime, especially nitrate particles were the major contributors in high $PM_{2.5}$ levels. In this section, we attempted to identify potential sources of airborne TN observed in the wintertime at the receptor site. To achieve this goal, stable nitrogen isotope ($\delta^{15}N$) has been employed to identify potential sources for nitrogen-containing compounds in the atmosphere (Savarino et al., 2013). Here, Bayesian isotope mixing model (SIAR, Stable Isotope Analysis in R) was attempted to quantitatively estimate the relative contributions of various sources to airborne TN.

During the winter sampling period, the average TN concentration was 18.7 ± 9.1 μg m^{-3} (ranging from 5.0 to 49.5 μg m^{-3}). NH_4^+-N

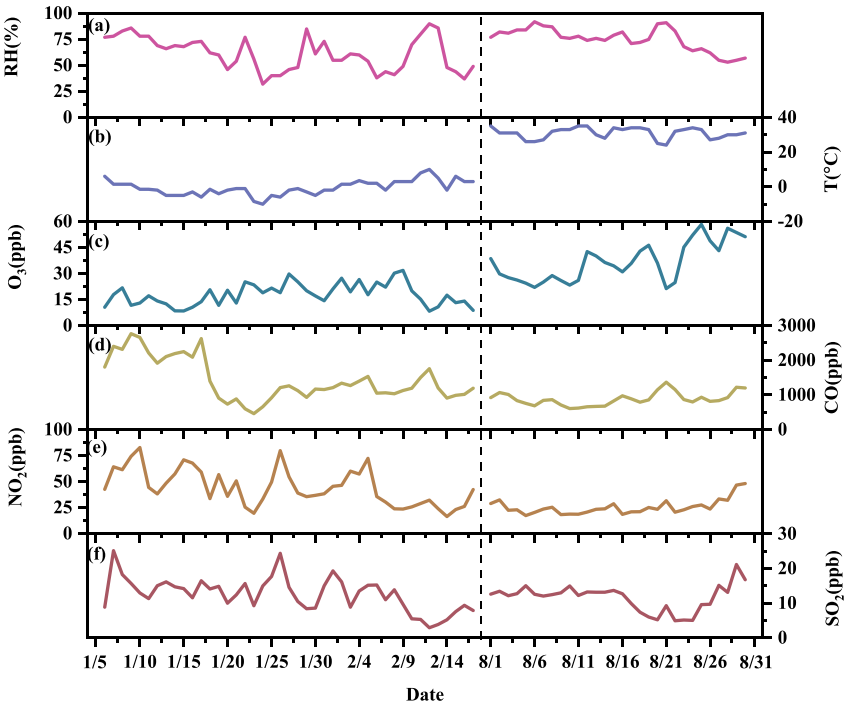

Fig. 3. Temporal variations of (a) RH, (b) T, and concentrations in (c) O_3, (d) CO, (e) NO_2, (f) SO_2 during the sampling periods.

dominated over the TN, which accounted for 62%, followed by NO_3^--N (29%) and organic nitrogen (ON) (9%) (see in Fig. 5). Since the compositions and formations of organic nitrogen are extremely complicated and cannot be easily identified, we focused on identifying the sources of inorganic nitrogen only. The $\delta^{15}N$ of TN varied from −1.3 to +13.2‰ with a mean value of 6.9 ± 3.6‰ during the wintertime. Previously, nitrogen isotope in urban polluted air in China has been investigated (Pan et al., 2018a,b; Chang et al., 2016; Wang et al., 2017). Our $\delta^{15}N$ value was a little heavier than that (2.8 ± 6.4‰) in Beijing, but much lighter than that (18.5 ± 5.8‰) at Menyuan (Wang et al., 2017), which is a representative of background atmosphere. The large difference of $\delta^{15}N$ of TN reflected that the sources of airborne TN were very distinct between urban and background areas.

To quantitatively estimate the source apportionments of airborne TN, the six dominant nitrogen sources served as input data in SIAR model. Table 3 listed the $\delta^{15}N$-NO_x and $\delta^{15}N$–NH_3 values for our selected sources. The $\delta^{15}N$-NO_x of coal combustion was 13.7 ± 4.6‰ (Felix et al., 2012, 2015; Walters et al., 2015c), the $\delta^{15}N$-NO_x of biomass burning was 1.0 ± 4.1‰ (Chang et al., 2018), while $\delta^{15}N$-NO_x of vehicle exhausts exhibited lighter $\delta^{15}N$ value of −7.3 ± 6.7‰ (Felix and Elliott, 2014; Heaton et al., 1997; Walters et al., 2015a). For $\delta^{15}N$–NH_3, combustion-related sources (including power plant, coal combustion and vehicle exhaust) had a mean $\delta^{15}N$ value of −14 ± 2.7‰ (Felix et al., 2013; Chang et al., 2016). The lighter $\delta^{15}N$–NH_3 values of −29.1 ± 1.7‰ and −37.8 ± 3.6‰ were found for animal wastes and urban volatilization (Chang et al., 2015, 2016).

The molar ratios between ambient NH_4^+ and (NO_3^- + 2 × SO_4^{2-}) averaged at 1.04, implying that there was residual NH_4^+ ions in aerosol phase after neutralizing by SO_4^{2-} and NO_3^-, indicating NH_4^+-rich regime. Consequently, N isotope fractionation would be occurred during the conversion of NH_3 to NH_4^+ (Wang et al., 2017). Prior estimating the potential sources of airborne particle TN, the isotope fractionation effect should be seriously considered (Wang et al., 2017; Heaton et al., 1997). To account for the effect of N isotope exchange, the $\delta^{15}N$–NH_4^+ arose from NH_3 to NH_4^+ can be calculated as (Pan et al., 2018a,b):

$$\delta^{15}\mathrm{N}-\mathrm{NH}_4^+ = \delta^{15}\mathrm{N}-\mathrm{NH}_3 + \varepsilon \times (1-f) \quad (5)$$

where $\delta^{15}N$–NH_4^+ is the $\delta^{15}N$ value of particulate NH_4^+ converted from initial NH_3. $\delta^{15}N$–NH_3 is the $\delta^{15}N$ value of initial NH_3 emitted directly from emission source. ε is the experimental isotope fractionation factor (33‰, Pan et al., 2018a,b); *f* is the molar ratio of particle NH_4^+ to total (NH_4^+ + NH_3) in the atmosphere. Thus, the N isotope fractionation factor ($\varepsilon_{NH3\leftrightarrow NH4+}$) was expressed as ε × (1-*f*) under the assumption of a well-mixed closed system (Pan et al., 2018a,b). In Eq. (5), *f* can be calculated by the concentrations of NH_3 and NH_4^+. We did not measure airborne NH_3 concentrations in this work and therefore we used ISORROPIA II to predict its concentration. Using the predicted NH_3 and observed NH_4^+ concentration, the *f* values were obtained with ranging from 0.52 to 0.81, resulting in the average N isotope fractionation factor ($\varepsilon_{NH3\leftrightarrow NH4+}$) of 13.8 ± 2.9‰ (see in Table S1). Subsequently, the $\delta^{15}N$–NH_3 values for each source should be plus $\varepsilon_{NH3\leftrightarrow NH4+}$ value before serving as input data for ISAR model.

Similarly, the isotopic exchange also occurred between NO_x and particle NO_3^- (Walters et al., 2016). The formation mechanisms of particle NO_3^- were distinct during daytime and nighttime. In the daytime, HNO_3 is mainly produced through the oxidation of NO_2 with OH radical. On the contrary, hydrolysis of N_2O_5 on water surface in the preexisting aerosols is a major pathway for HNO_3 production. When nitric acid transforms to particulate nitrate, fractionations of isotopes would be occurred. Recently, Chang et al. (2018) used a modified approach to estimate the N isotope fractionation from NO_x to HNO_3 (NO_3^-) in urban polluted air. Here, we adopted the same method to calculate the N isotope fractionation during the conversion of gas NO_x to particle NO_3^- ($\varepsilon_{NOx\leftrightarrow NO3-}$). Briefly, $\varepsilon_{NOx\leftrightarrow NO3-}$ was affected by two N isotope exchange reactions:

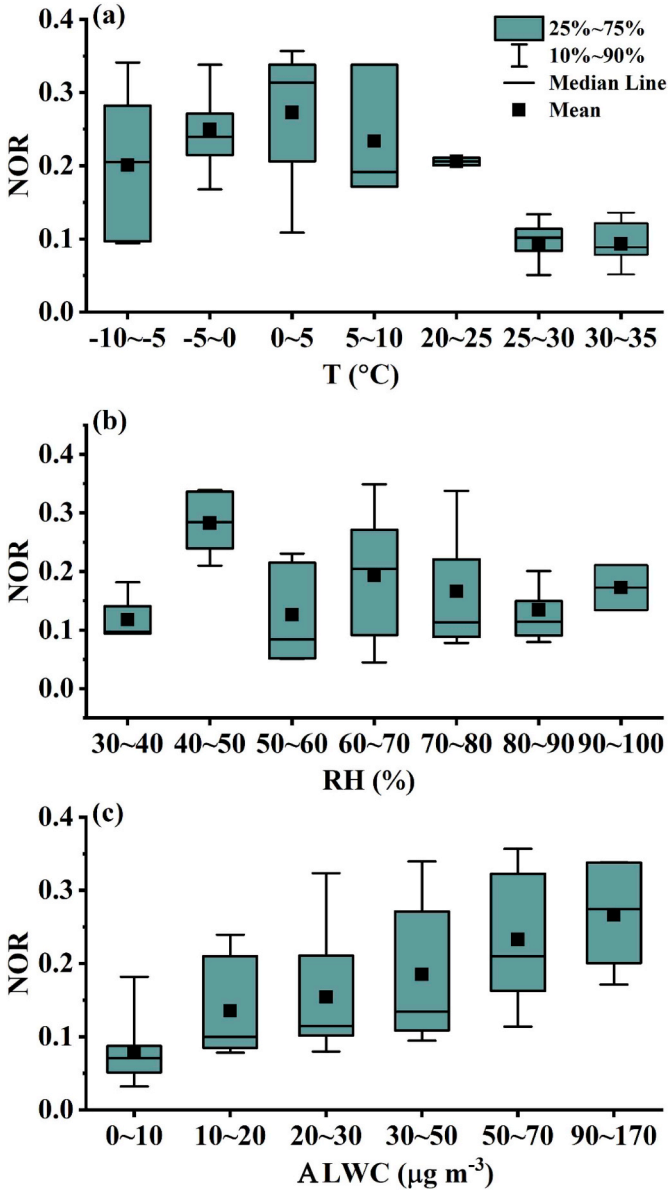

Fig. 4. NOR values dependent on various (a) T, (b) RH, and (c) ALWC.

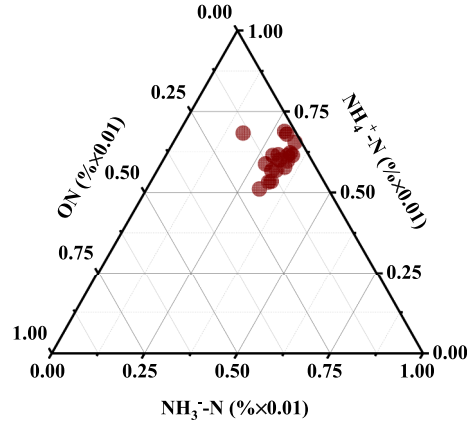

Fig. 5. Ternary diagram for the ratio of NH_4^+-N, NO_3–N and ON in $PM_{2.5}$ in the winter.

$$\varepsilon_{NO_x\leftrightarrow NO_3^-} = \gamma \times \varepsilon_{N_{(NO_x\leftrightarrow pNO_3^-)_{OH}}} + (1-\gamma) \times \varepsilon_{N_{(NO_x\leftrightarrow pNO_3^-)_{H_2O}}}$$

$$= \gamma \times \varepsilon_{N_{(NO_x\leftrightarrow pHNO_3)_{OH}}} + (1-\gamma) \times \varepsilon_{N_{(NO_x\leftrightarrow pHNO_3)_{H_2O}}}$$

$$= \gamma \times 1000 \times \left[\frac{(15\alpha_{NO_2/NO} - 1)(1-f_{NO_2})}{(1-f_{NO_2}) + (15\alpha_{NO_2/NO} \times f_{NO_2})}\right] + \left(1-\gamma\right) \times 1000 \times \left(15\alpha_{N_2O_5/NO_2} - 1\right) \quad (6)$$

$$15\alpha X/Y - 1 = \frac{1}{1000} \times \left(\frac{A}{T^4} \times 1010 + \frac{B}{T3} \times 10^8 + \frac{C}{T2} \times 10^6 + \frac{D}{T} \times 104\right) \quad (7)$$

Where γ is the contribution from isotope fractionation through the reaction of NO_x and photochemically produced OH to yield HNO_3 (pNO_3^-) with a range from 0 to 1; f_{NO2} represents the ratio of NO_2 to NO_x, ranging from 0.2 to 0.95 (Walters and Michalski, 2015); $^{15}\alpha_{NO2/NO}$ and $^{15}\alpha_{N2O5/NO2}$ are the equilibrium N isotope fractionation factors between NO (N_2O_5) and NO_2 which depends on atmosphere temperature only. Parameters of A, B, C and D are experimental constants with the temperature range of 150–450 K (Table S2) (Walters and Michalski, 2015b; Walters et al., 2016; Zong et al., 2017). According to the Eq. (7), we obtained the values of $^{15}\alpha_{NO2/NO}$ and $^{15}\alpha_{N2O5/NO2}$ based on the atmospheric temperature (K). And then the average value of $\varepsilon_{NOx\leftrightarrow NO3-}$ could be calculated through Eq. (6) under certain condition of f_{NO2} and γ (an example was showed in Table S3). Due to the wide range of f_{NO2} and γ, we calculated several times under the different situations of f_{NO2} (0.2, 0.3, 0.4, 0.5, 0.6, 0.7, 0.8, 0.9, 0.95) and γ (0, 0.1, 0.2, 0.3, 0.4, 0.5, 0.6, 0.7, 0.8, 0.9, 1) and the results showed that $\varepsilon_{NOx\leftrightarrow NO3-}$ had a widely range from 2.0‰ ($\gamma = 1$, $f_{NO2} = 0.95$) to 30.4‰ ($\gamma = 1$, $f_{NO2} = 0.2$) with the average value of 9.1 ± 7.0‰ (Table S4), suggested N isotope fractionation decreased obviously with increasing ratio of NO_2 to NO_x. Before input the $\delta^{15}N$ of each source in Table 3 to the model, we considered the fractionation effect between NO_x (NH_3) and NO_3^- (NH_4^+) by adding the average value of 9.1 ± 7.0‰ (13.8 ± 2.9‰) to the $\delta^{15}N$ isotope values of NO_x (NH_3) emitted from each selected emission. Then the $\delta^{15}N$ values of vehicle exhausted ($\delta^{15}N$–NO_3^-: 1.8 ± 9.7‰), coal combustion of $\delta^{15}N$–NO_3^- (22.8 ± 8.3‰), biomass burning of $\delta^{15}N$–NO_3^- (10.1 ± 8.1‰), urban volatilization of $\delta^{15}N$–NH_4^+ (−23.9 ± 4.6‰), animal waste of $\delta^{15}N$–NH_4^+ (−15.2 ± 3.4‰), and combustion-related sources of $\delta^{15}N$–NH_4^+ (−0.1 ± 4.0‰) were used to do analyze TN sources.

The corrected $\delta^{15}N$ values in emission sources and $\delta^{15}N$ for ambient TN then served as input data of SIAR model to estimate the source apportionments of TN in the $PM_{2.5}$. Here, we optimized SIAR model by adding a restrictive criterion, that is, the percentages estimated 10 thousand times and retain the values between the maximum and minimum values of the molar ratio of ammonia nitrogen to nitrate nitrogen as followed:

$$\frac{[NH_4^+ - N]}{[NO_3^- - N]}\min < \frac{P(NH_3)1 + P(NH_3)2 + \ldots + P(NH_3)i}{P(NO_x)1 + P(NO_x)2 + \ldots + P(NO_x)j} < \frac{[NH_4^+ - N]}{[NO_3^- - N]}\max \quad (8)$$

where $[NH_4^+$-N$]/[NO_3^-$-N$]_{min}$ and $[NH_4^+$-N$]/[NO_3^-$-N$]_{max}$ are the minimum and maximum values of the molar mass proportions of observed ammonium nitrogen and nitrate nitrogen in this field measurements; $P(_{NH3})$ and $P(_{NOx})$ are the proportions of the different sources of NH_3 and NO_x estimated by SIAR model; i is the number of sources of NH_3, and j is the number of sources of NO_x. The range of $[NH_4^+$-N$]/[NO_3^-$-N] was 1.3–3.9 with the average value of 2.1 ± 0.6. Thus, the values of $[NH_4^+$-N$]/[NO_3^-$-N$]_{min}$ and $[NH_4^+$-N$]/[NO_3^-$-N$]_{max}$ in Eq. (8) were 1.3 and 3.9, respectively. In this work, we estimated potential sources of nitrogen-containing aerosols through SIAR model without

Table 3
Statistic of δ^{15}N-NO_x and δ^{15}N–NH_3 in various sources of bulk N reported in previous studies.

Source types	N species	δ^{15}N (‰)	References
Coal combustion	NO_x	13.72 ± 4.57	Felix et al. (2012, 2015); Walters et al. (2015)
Vehicle exhausts	NO_x	−7.25 ± 6.69	Felix and Elliott (2014); Heaton et al. (1997); Walters et al. (2015)
Biomass burning	NO_x	1.04 ± 4.13	Chang et al. (2018)
Animal wastes	NH_3	−29.1 ± 1.7	Chang et al. (2016)
Combustion-related sources	NH_3	−14 ± 2.7	Felix et al. (2013); Chang et al. (2016)
Urban volatilization	NH_3	−37.8 ± 3.6	Chang et al. (2015); Chang et al. (2016)

Table 4
Comparison of the results between the original and optimized SIAR model.

Sources appointment	Original output	Optimized output
	Mean ± std	Mean ± std
NO_x from coal combustion	30 ± 7%	33 ± 5%
NO_x from vehicle exhausts	15 ± 9%	3 ± 3%
NO_x from biomass burning	22 ± 10%	5 ± 5%
NH_3 from animal wastes	8 ± 6%	6 ± 6%
NH_3 from combustion-related sources	18 ± 10%	49 ± 7%
NH_3 from urban volatilization	6 ± 4%	3 ± 2%

(original output) and with (optimized output) restrictive conditions as listed in Table 4. Significant differences of output values for results were found from the original and optimized SIAR model. This suggested that estimation potential sources of N containing aerosols through SIAR model with restrictions enhanced the accuracy and is therefore needed.

Fig. 6 shows the estimated contributions of potential nitrogen sources to the TN in $PM_{2.5}$ at the sampling site in the wintertime. As illustrated, NH_3 (P_{NH3}) emissions contributed 59% to particle TN while NO_x (P_{NOx}) contributed to 41% during the wintertime sampling period. The mean ratios of P_{NH3} to P_{NOx} was 1.4 ± 0.1, which was consistent with the observed molar ratio of NH_4^+-N to NO_3^--N. According to the estimations, NH_3 from combustion-related sources contributed 49% to particulate TN, which was the most predominant source followed by NO_x derived from coal combustion (33%), NH_3 from animal wastes (6%), NO_x from biomass burning (5%), NH_3 from urban volatilization (3%) and NO_x derived from vehicle exhausts (3%). As a result, coal combustion related sources seemed to be the predominant source of particulate TN in the urban city. The limitation of this research was that we did not consider the influence of ON, so results existed a certain uncertainty. In the future, we need to improve the technical method to take this part into account.

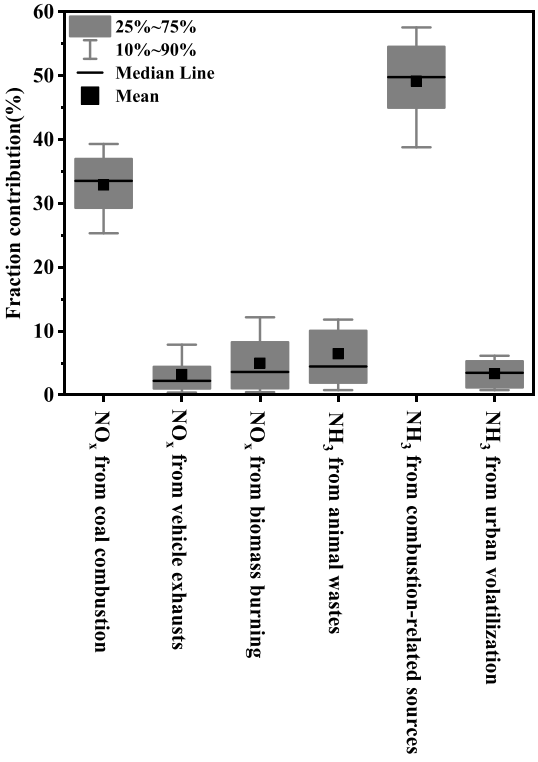

Fig. 6. Relative contributions of potential nitrogen sources to airborne $PM_{2.5}$ TN at Xuzhou during the wintertime.

4. Conclusion

In this work, $PM_{2.5}$ samples were collected in Xuzhou in the wintertime and summertime, respectively. The $PM_{2.5}$ concentrations ranged from 35 to 351 μg m^{-3}, with a mean value of 137 ± 88 μg m^{-3}. Water soluble ions accounted 30% for $PM_{2.5}$ mass with SO_4^{2-} being the most predominant species, followed by NO_3^- and NH_4^+. The abundance of TN, consists mainly of NH_4^+-N and NO_3^--N, in $PM_{2.5}$ was 8%. Compared to the concentrations in the summertime, all species revealed high levels in the wintertime. During the high $PM_{2.5}$ days, enhancement of TN was mainly attributed to nitrate aerosols, which might produce by heterogeneous reaction since NOR correlated well with ALWC. This valuable data can give hints for potential sources of particulate TN. The results showed that δ^{15}N in TN varied from −1.3 to +13.2‰ with a mean value of 6.9 ± 3.6‰. Coupling the optimized SIAR model and nitrogen isotope values, potential sources of TN in $PM_{2.5}$ were assessed. We highlighted that control of NH_3 emissions from combustion-related emissions and animal waste along with NO_x from coal combustion might be an important way to reduce $PM_{2.5}$ levels. The method and results from this study may be applied in both developed and emerging regions with different pollution levels.

While this study provided a simple and fast approach to quantify the sources of nitrogen-containing aerosol, there were still considerable uncertainties due to the complex N isotope fractionation during chemical conversion (i.e., NO_x (NH_3) to NO_3^- (NH_4^+)). Although we got the fractionation factors of NO_x (NH_3) ↔ NO_3^- (NH_4^+) by theoretical calculation and the uncertainty was reduced by the constraint condition, a deviation between calculated and the actual fractionation values may still exist. We recommend future concurrent observations of NO_x (NH_3) and NO_3^- (NH_4^+) isotopes to reduce these uncertainties.

Declaration of interests

The authors declare that they have no known competing financial interests or personal relationships that could have appeared to influence the work reported in this paper.

The authors declare the following financial interests/personal relationships which may be considered as potential competing interests:

Acknowledgments

This study was financially supported by the National Key R&D Program of China (Grant No. 2017YFC0212704), the Natural Scientific Foundation of China (No. 91644103 and 41603104), the Provincial Natural Science Foundation of Jiangsu (Grant No. BK20180040) and the funding of Jiangsu Innovation & Entrepreneurship Team.

Appendix A. Supplementary data

Supplementary data to this article can be found online at https://doi.org/10.1016/j.atmosenv.2019.05.020.

References

Aggarwal, S.G., Kawamura, K., Umarji, G.S., Tachibana, E., Patil, R.S., Gupta, P.K., 2012. Organic and inorganic markers and stable C-, N-isotopic compositions of tropical coastal aerosols from megacity Mumbai: sources of organic aerosols and atmospheric processing. Atmos. Chem. Phys. 13, 20593–20630.

Bian, Y.X., Zhao, C.S., Ma, N., Chen, J., Xu, W.Y., 2014. A study of aerosol liquid water content based on hygroscopicity measurements at high relative humidity in the North China Plain. Atmos. Chem. Phys. 14, 6417–6426.

Booth, B., Bellouin, N., 2015. Climate change: black carbon and atmospheric feedbacks. Nature 519, 167–168.

Cao, C., Jiang, W., Wang, B., Fang, J., Lang, J., Tian, G., Jiang, J., Zhu, T., 2014. Inhalable microorganisms in Beijing's $PM_{2.5}$ and PM_{10} pollutants during a severe smog event. Environ. Sci. Technol. 48, 1499–1507.

Chang, Y., Ma, H., 2016. Comment on "fossil fuel combustion-related emissions dominate atmospheric ammonia sources during severe haze episodes: evidence from ^{15}N-stable isotope in size-resolved aerosol ammonium. Environ. Sci. Technol. 50 19765-10766.

Chang, Y., Deng, C., Dore, A.J., Zhuang, G., 2015. Human excreta as a stable and important source of atmospheric ammonia in the megacity of Shanghai. PLoS One 10, e0144661.

Chang, Y., Zhang, Y., Tian, C., Zhang, S., Ma, X., Cao, F., Liu, X., Zhang, W., Kuhn, T., Lehmann, M.F., 2018. Nitrogen isotope fractionation during gas-to-particle conversion of NO_x to NO_3 in the atmosphere–implications for isotope-based NO_x source apportionment. Atmos. Chem. Phys. 18, 11647–11661.

Che, H., Xia, X., Zhu, J., Li, Z., Dubovik, O., Holben, B., Goloub, P., Chen, H., Estelles, V., Cuevas-Agulló, E., Blarel, L., Wang, H., Zhao, H., Zhang, X., Wang, Y., Sun, J., Tao, R., Zhang, X., Shi, G., 2014. Column aerosol optical properties and aerosol radiative forcing during a serious haze-fog month over North China Plain in 2013 based on ground-based sunphotometer measurements. Atmos. Chem. Phys. 14, 2125–2138.

Cheng, Y., Zheng, G., Wei, C., Mu, Q., Zheng, B., Wang, Z., Gao, M., Zhang, Q., He, K., Carmichael, G., Pöschl, U., Su, H., 2016. Reactive nitrogen chemistry in aerosol water as a source of sulfate during haze events in China. Adv. Sci. 2, e1601530.

Cheng, Z., Wang, S., Qiao, L., Wang, H., Zhou, M., Fu, X., Lou, S., Luo, L., Jiang, J., Chen, C., Wang, X., Hao, J., 2017. Insights into extinction evolution during extreme low visibility events: case study of Shanghai, China. Sci. Total Environ. 618, 793–803.

Evans, J.S., Handley, S.J., Perham, N., Over, D.E., Thompson, V.A., 2000. Frequency versus probability formats in statistical word problems. Cognition 77, 197–213.

Felix, J.D., Elliott, E.M., 2014. Isotopic composition of passively collected nitrogen dioxide emissions: vehicle, soil and livestock source signatures. Atmos. Environ. 92, 359–366.

Felix, J.D., Elliott, E.M., Shaw, S.L., 2012. Nitrogen isotopic composition of coal-fired power plant NO_x: influence of emission controls and implications for global emission inventories. Environ. Sci. Technol. 46, 3528–3535.

Felix, J.D., Elliott, E.M., Avery, G.B., Avery, G.B., Kieber, R.J., Mead, R.N., Willey, J.D., Mullaugh, K.M., 2015. Isotopic composition of nitrate in sequential Hurricane Irene precipitation samples: implications for changing NO_x sources. Atmos. Environ. 106, 191–195.

Felix, J.D., Elliott, E.M., Gish, T.J., McConnell, L.L., Shaw, S.L., 2013. Characterizing the isotopic composition of atmospheric ammonia emission sources using passive samplers and a combined oxidation-bacterial denitrifier approach. Rapid Commun. Mass Spectrom. 27, 2239–2246.

Fountoukis, C., Nenes, A., 2007. ISORROPIA II: a computationally efficient thermodynamic equilibrium model for K^+–Ca^{2+}–Mg^{2+}–NH_4^+–Na^+–SO_4^{2-}–NO_3^-–Cl^-–H_2O aerosols. Atmos. Chem. Phys. 7, 4639–4659.

Guo, H., Xu, L., Bougiatioti, A., Cerully, K.M., Capps, S.L., Hite, J.R., Carlton, A.G., Lee, S.-H., Bergin, M.H., Ng, N.L., Nenes, A., Weber, R.J., 2015. Particle water and pH in the southeastern United States. Atmos. Chem. Phys. Discuss. 14, 27143–27193.

Heaton, T.H., Spiro, B., Robertson, S.M., 1997. Potential canopy influences on the isotopic composition of nitrogen and sulphur in atmospheric deposition. Oecologia 109, 600–607.

Hegde, P., Kawamura, K., Joshi, H., Naja, M., 2016. Organic and inorganic components of aerosols over the central Himalayas: winter and summer variations in stable carbon and nitrogen isotopic composition. Environ. Sci. Pollut. Res. 23, 6102–6118.

Jiang, Y., Zhuang, G., Wang, Q., Huang, K., Deng, C., Yu, G., Xu, C., Fu, Q., Lin, Y., Fu, J.S., Li, M., Zhou, Z., 2018. Impact of mixed anthropogenic and natural emissions on air quality and eco-environment—the major water-soluble components in aerosols from northwest to offshore isle. Air Qual. Atmos. Health 11, 521–534.

Kawashima, H., Kurahashi, T., 2011. Inorganic ion and nitrogen isotopic compositions of atmospheric aerosols at Yurihonjo, Japan: implications for nitrogen sources. Atmos. Environ. 45, 6309–6316.

Li, X., Zhang, R., Cong, X., Cheng, L., Liu, J., Xu, H., 2015. Characterization of the size-segregated inorganic compounds in Lin'an, a regional atmosphere background station in the Yangtze river delta region. Atmos. Pollut. Res. 6, 1058–1065.

Li, Y.J., Sun, Y., Zhang, Q., Li, X., Zhou, Z., Chan, C.K., 2017. Real-time chemical characterization of atmospheric particulate matter in China: a review. Atmos. Environ. 158, 270–304.

Liang, L., Engling, G., Zhang, X., Sun, J., Zhang, Y., Xu, W., Liu, C., Zhang, G., Liu, X., Ma, Q., 2017. Chemical characteristics of $PM_{2.5}$, during summer at a background site of the Yangtze River Delta in China. Atmos. Res. 198, 163–172.

Lin, Y.C., Cheng, M.T., 2007. Evaluation of formation rates of NO_2, to gaseous and particulate nitrate in the urban atmosphere. Atmos. Environ. 41, 1903–1910.

Lin, Z.J., Zhang, Z.S., Zhang, L., Tao, J., Zhang, R.J., Cao, J.J., Fan, S.J., Zhang, Y.H., 2014. An alternative method for estimating hygroscopic growth factor of aerosol light-scattering coefficient: a case study in an urban area of Guangzhou, South China. Atmos. Chem. Phys. 14, 7631–7644.

Ming, L., Ling, J., Li, J., Fu, P., Yang, W., Liu, D., Zhang, G., Wang, Z., Li, X., 2017. $PM_{2.5}$, in the Yangtze River Delta, China: chemical compositions, seasonal variations, and regional pollution events ☆. Environ. Pollut. 223, 200–212.

Mukherjee, A., Agrawal, M., 2017. A global perspective of fine particulate matter pollution and its health effects. Rev. Environ. Contam. Toxicol. 244, 5–51.

Ouyang, Y., 2013. China wakes up to the crisis of air pollution. Lancet Respir. Med. 1, 12.

Pan, Y., Tian, S., Liu, D., Fang, Y., Zhu, X., Gao, M., Gao, J., Michalski, G., Wang, T., 2018a. Isotopic evidence for enhanced fossil fuel sources of aerosol ammonium in the urban atmosphere. Environ. Pollut. 238, 942–947.

Pan, Y., Wang, Y., Zhang, J., Liu, Z., Wang, L., Tian, S., Tang, G., Gao, W., Ji, D., Song, T., Wang, Y., 2016. Redefining the importance of nitrate during haze pollution to help optimize an emission control strategy. Atmos. Environ. 141, 197–202.

Pan, Y., Tian, S., Liu, D., Fang, Y., Zhu, X., Gao, M., Wentworth, G.,R., Michalski, G., Huang, X., Wang, Y., 2018b. Source apportionment of aerosol ammonium in an ammonia-rich atmosphere: an isotopic study of summer clean and hazy days in urban Beijing. J. Geophys. Res.: Atmosphere 123, 5681–5689.

Parnell, A.C., Inger, R., Bearhop, S., Jackson, A.L., 2010. Source partitioning using stable isotopes: coping with too much variation. PLoS One 5, e9672.

Pathak, R.K., Wu, W.S., Wang, T., 2009. Summertime $PM_{2.5}$ ionic species in four major cities of China: nitrate formation in an ammonia-deficient atmosphere. Atmos. Chem. Phys. 8, 11487–11517.

Peplow, M., 2014. Beijing smog contains witches' brew of microbes. Nature. https://doi.org/10.1038/nature.2014.14640.

Petäjä, T., Järvi, L., Kerminen, V.-M., Ding, A.J., Sun, J.N., Nie, W., Kujansuu, J., Virkkula, A., Yang, X., Fu, C.B., Zilitinkevich, S., Kulmala, M., 2016. Enhanced air pollution via aerosol-boundary layer feedback in China. Sci. Rep. 6, 18998.

Pósfai, M., Simonics, R., Li, J., Hobbs, P.V., Buseck, P.R., 2003. Individual aerosol particles from biomass burning in southern Africa: 1. Compositions and size distributions of carbonaceous particles. J. Geophys. Res. Atmos. 108, 8483.

Savarino, J., Morin, S., Erbland, J., Grannec, F., Patey, M.D., Vicars, W., Alexander, B., Achterberg, E.P., 2013. Isotopic composition of atmospheric nitrate in a tropical marine boundary layer. Proc. Natl. Acad. Sci. U.S.A. 110, 17668–17673.

Sulong, N.A., Latif, M.T., Khan, M.F., Amil, N., Ashfold, M.J., Wahab, M.I.A., Chan, K.M., Sahani, M., 2017. Source apportionment and health risk assessment among specific age groups during haze and non-haze episodes in Kuala Lumpur, Malaysia. Sci. Total Environ. 601–602, 556–570.

Sun, Y., Chen, C., Zhang, Y., Xu, W., Zhou, L., Cheng, X., Zheng, H., Ji, D., Li, J., Tang, X., Fu, P., Wang, Z., 2016. Rapid formation and evolution of an extreme haze episode in Northern China during winter 2015. Sci. Rep. 6, 27151.

Taghvaee, S., Sowlat, M.H., Mousavi, A., Hassanvand, M.S., Yunesian, M., Naddafi, K., Sioutas, C., 2018. Source apportionment of ambient $PM_{2.5}$ in two locations in central Tehran using the Positive Matrix Factorization (PMF) model. Sci. Total Environ. 628–629, 672–686.

Tan, T., Hu, M., Li, M., Guo, Q., Wu, Y., Fang, X., Gu, F., Wang, Y., Wu, Z., 2018. New insight into $PM_{2.5}$ pollution patterns in Beijing based on one-year measurement of chemical compositions. Sci. Total Environ. 621, 734–743.

Tao, J., Zhang, Z., Tan, H., Zhang, L., Wu, Y., Sun, J., Che, H., Cao, J., Cheng, P., Chen, L., Zhang, R., 2018. Observational evidence of cloud processes contributing to daytime elevated nitrate in an urban atmosphere. Atmos. Environ. 186, 209–215.

Walters, W.W., Goodwin, S.R., Michalski, G., 2015a. Nitrogen stable isotope composition (delta N-15) of vehicle-emitted NO_x. Environ. Sci. Technol. 49, 2278–2285.

Walters, W.W., Michalski, G., 2015. Theoretical calculation of nitrogen isotope equilibrium exchange fractionation factors for various NO*y* molecules. Geochem. Cosmochim. Acta 164, 284–297.

Walters, W.W., Tharp, B.D., Fang, H., Kozak, B.J., Michalski, G., 2015c. Nitrogen isotope composition of thermally produced NO_x from various fossil-fuel combustion sources. Environ. Sci. Technol. 49, 11363–11371.

Walters, W.W., Simonini, D.S., Michalski, G., 2016. Nitrogen isotope exchange between NO and NO_2 and its implications for $\delta^{15}N$ variations in tropospheric NO_x and atmospheric nitrate. Geophys. Res. Lett. 43, 440–448.

Wang, H., An, J., Cheng, M., Shen, M., Shen, L., Zhu, B., Li, Y., Wang, Y., Duan, Q., Sullivan, A., Xia, L., 2016. One year online measurements of water-soluble ions at the industrially polluted town of Nanjing, China: sources, seasonal and diurnal variations. Chemosphere 148, 526–536.

Wang, Y.L., Liu, X.Y., Song, W., Yang, W., Han, B., Dou, X.Y., Zhao, X.D., Song, Z.L., Liu, C.Q., Bai, Z.P., 2017. Source appointment of nitrogen in $PM_{2.5}$ based on bulk $\delta^{15}N$ signatures and a Bayesian isotope mixing model. Tellus B: Chem. Phys. Meteorol. 69, 1299672.

Wang, Y., Zhang, R., Saravanan, R., 2014. Asian pollution climatically modulates mid-latitude cyclones following hierarchical modelling and observational analysis. Nat. Commun. 5, 3098.

Wu, J., Xu, C., Wang, Q., Cheng, W., 2016. Potential sources and formations of the $PM_{2.5}$ pollution in urban Hangzhou. Atmosphere 7, 100.

Xu, J., Xu, M., Snape, C., He, J., Behera, S.N., Xu, H.H., Ji, D.S., Wang, C.J., Yu, H., Xiao, H., Jiang, Y.J., Qi, B., Du, R.G., 2017a. Temporal and spatial variation in major ion chemistry and source identification of secondary inorganic aerosols in Northern Zhejiang Province, China. Chemosphere 179, 316–330.

Xu, L., Duan, F., He, K., Ma, Y., Zhu, L., Zheng, Y., Huang, T., Kimoto, T., Ma, T., Li, H., Ye, S., Yang, S., Sun, Z., 2017b. Characteristics of the secondary water-soluble ions in a typical autumn haze in Beijing. Environ. Pollut. 227, 296–305.

Xue, J., Yuan, Z., Griffith, S.M., Yu, X., Lau, A.K., Yu, J.Z., 2016. Sulfate formation enhanced by a cocktail of high NO_x, SO_2, particulate matter, and droplet pH during haze-fog events in megacities in China: an observation-based modeling investigation. Environ. Sci. Technol. 50, 7325–7334.

Yang, S., Ma, Y.L., Duan, F.K., He, K.B., Wang, L.T., Wei, Z., Zhu, L.D., Ma, T., Li, H., Ye, S.Q., 2017. Characteristics and formation of typical winter haze in Handan, one of the most polluted cities in China. Sci. Total Environ. 30 (613–614), 1367–1375.

Zhang, G., Xu, H., Qi, B., Du, R., Gui, K., Wang, H., Jiang, W., Liang, L., Xu, W., 2018. Characterization of atmospheric trace gases and particulate matter in Hangzhou, China. Atmos. Chem. Phys. 18, 1705–1728.

Zhang, Q., Ma, X., Tie, X., Huang, M., Zhao, C., 2009. Vertical distributions of aerosols under different weather conditions: analysis of in-situ aircraft measurements in Beijing, China. Atmos. Environ. 43, 5526–5535.

Zhang, T., Chillrud, S.N., Ji, J., Chen, Y., Pitiranggon, M., Li, W., Liu, Z., Yan, B., 2017. Comparison of $PM_{2.5}$ exposure in hazy and non-hazy days in Nanjing, China. Aerosol Air Qual. Res. 17, P2235–P2246.

Zong, Z., Wang, X., Tian, C., Chen, Y., Fang, Y., Zhang, F., Li, C., Sun, J., Li, J., Zhang, G., 2017. First assessment of NO_x sources at a regional background site in North China using isotopic analysis linked with modeling. Environ. Sci. Technol. 51, 5923–5931.